Hindawi
Wireless Communications and Mobile Computing
Volume 2022, Article ID 8209256, 10 pages
https://doi.org/10.1155/2022/8209256

Research Article

Realistic Prognostic Modeling of Specific Attenuation due to Rain at Microwave Frequency for Tropical Climate Region

Joseph Isabona,[1] Agbotiname Lucky Imoize,[2,3] Paresh Rawat,[4] Sajjad Shaukat Jamal,[5] Bhasker Pant,[6] Stephen Ojo,[7] and Simon Karanja Hinga[8]

[1]*Department of Physics, Federal University Lokoja, P.M.B., 1154 Lokoja, Nigeria*
[2]*Department of Electrical and Electronics Engineering, Faculty of Engineering, University of Lagos, Akoka, Lagos 100213, Nigeria*
[3]*Department of Electrical Engineering and Information Technology, Institute of Digital Communication, Ruhr University, 44801 Bochum, Germany*
[4]*S. N. Technology, Bhopal, India*
[5]*Department of Mathematics, College of Science, King Khalid University, Abha, Saudi Arabia*
[6]*Department of Computer Science & Engineering, Graphic Era Deemed to be University, Dehradun, Uttarakhand 248002, India*
[7]*Department of Electrical and Computer Engineering, College of Engineering, Anderson University, Anderson, SC 29621, USA*
[8]*Department of Electrical and Electronic Engineering, Technical University of Mombasa, Mombasa, Kenya*

Correspondence should be addressed to Simon Karanja Hinga; kahinga@tum.ac.ke

Received 17 February 2022; Revised 16 March 2022; Accepted 29 March 2022; Published 14 April 2022

Academic Editor: Mohammad Farukh Hashmi

Absorption and scattering of propagated microwave radio signals by atmospheric variables, particularly rainfall, remained a major cause of propagation attenuation losses and service quality degradation over terrestrial communication links. The International Telecommunications Union Radio (ITU-R) reports and other related works in the literature provided information on attenuation due to rain and microwave propagation data. Such propagation attenuation information in the tropical region of Nigeria is destitute, especially at lower radio waves transmission frequencies. Therefore, this study addresses this problem by employing 12-year rainfall datasets to conduct realistic prognostic modeling of rain rate intensity levels. A classification of the rainfall data into three subgroups based on the depth of rainfall in the region is presented. Additionally, an in-depth estimation of specific rain attenuation intensities based on the 12-year rainfall data at 3.5 GHz is demonstrated. On average, the three rainfall classes produced rain rates of about 29.27 mm/hr, 73.71 mm/hr, and 105.39 mm/hr. The respective attenuation values are 0.89 dB, 1.71 dB, and 2.13 dB for the vertical polarisation and 1.09 dB, 1.20 dB, and 2.78 dB for the horizontal polarisation at 0.01% time percentage computation. Generally, results indicate that higher rain attenuation of 12% is observed for the horizontal polarisation compared to the vertical polarisation. These results can provide valuable first-hand information for microwave radio frequency planning in making appropriate decisions on attenuation levels due to different rainfall depths, especially for lower frequency arrays.

1. Introduction

In designing and deploying meaningful Earth-space terrestrial radio and microwave network-based communication systems, several attenuation effects owing to different atmospheric conditions need to be examined [1, 2]. The effects due to scattering, absorption, and depolarization by hydrometeors (e.g., snow, ice, sleet, and water droplets in clouds, precipitation, etc.) and atmospheric gases are considered at different transmission frequencies around the 11 GHz band [3, 4]. Due to heavy rainfall depth and fade, attenuation can damage signal propagation and reception at the user terminal [5, 6]. It can also cause short-term and long-term impairments in radio signal communication links [7–9]. Adverse atmospheric weather conditions (bad weather) due to different raindrops can absorb microwave-range signals

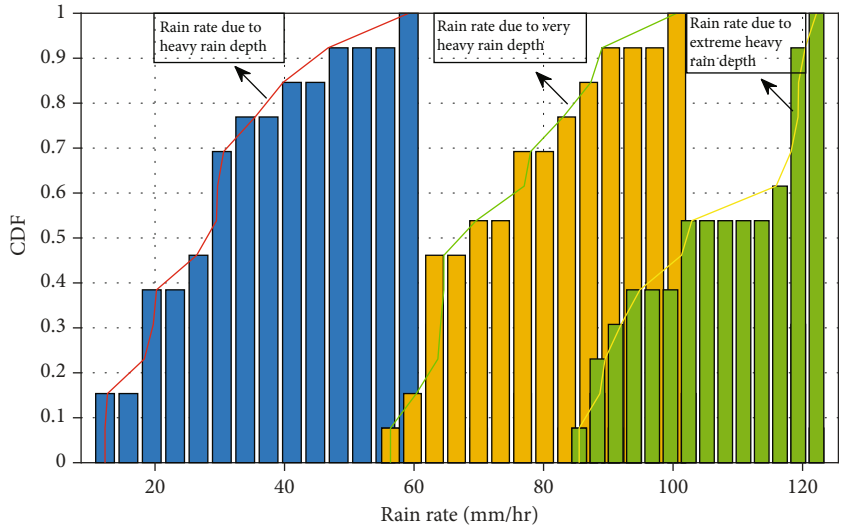

Figure 1: CDF statistical distribution of rain rates due to different rainfall depth.

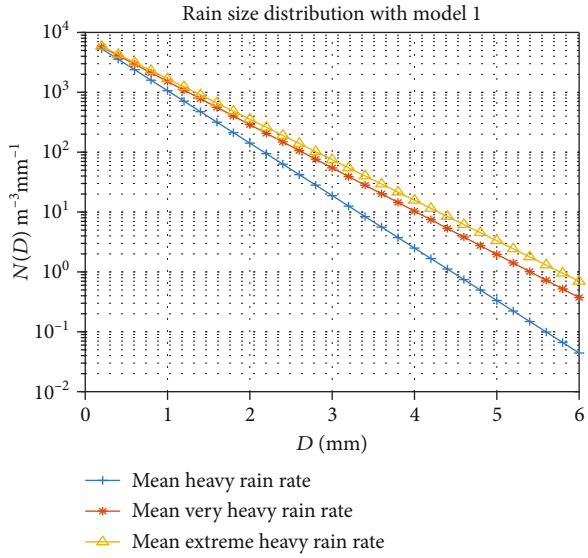

Figure 2: Raindrop size distribution evaluation with model 1.

in both terrestrial point-to-point and Earth-space satellite communication systems [10–13]. Thus, resulting in substantial path loss and severe degradation in signal coverage and quality of service [14–21]. In order to address this problem, estimating rain rate attenuation will enable terrestrial radio and microwave network planners to determine the type of diversity techniques to explore to combat or compensate for it during and after antenna deployment [22–25].

The knowledge of specific attenuation influenced by different rainfall drop sizes/depths and other weather-related issues is essential for efficient fade management processes. For instance, predictive quantification of rainfall attenuation impacts is critical to determining the requisite tracking speediness of fade moderation. The atmospheric earth surface comprises different layers with different characteristic features, properties, and structures. The troposphere, a vital component of the homosphere, is the most crucial sublayer for radio frequency engineers handling space terrestrial radio channels [26–28]. Studies on hydrometeors impacts, mainly due to rainfall intensity on propagated electromagnetic signal waves in recent decades, have been reported. Results indicate enormous path loss owing to high traffic and congestion issues in terrestrial cellular communication networks operating at lower higher frequency bands [22].

Several reports on rain attenuation impacts on communication systems are detailed in [22, 29–36]. In particular, the work in [29] presented a predictive analysis of rainfall attenuation and their probable influence on propagated microwaves for Uttarakhand, a tropical region in India. Similar rain attenuation modeling, but based on practical measurements of different rainfall drop sizes, is reported in [30] for the same region. Predictive analysis of rain attenuation and rain rate for satellite-based communication using TURKSAT in the Ku Band Beacon has been investigated [31]. Rain attenuation studies at microwave propagation frequencies over Malaysia environment using ITU-R, Ajayi model, and Global Crane Model are presented in [32]. The authors [33, 34] provide detailed rainfall attenuation distribution statistics over the wireless link at a higher microwave frequency in Japan and Korean territories. Specific practical attenuation measurement and modeling-based investigation approaches to rainfall intensity effects conducted in different countries are presented [35–44].

In recent literature, reconfigurable intelligent surface-(RIS-) based techniques for mitigating interference are gaining widespread popularity. RIS has been a candidate technology for the beyond 5G and 6G wireless networks. RISs can help improve the efficiency and performance of wireless communication networks [45, 46]. RISs are designed with passive materials to tackle interference in harsh and unfriendly environments [47]. In RIS deployment, wireless signals are transmitted from the transmitter to the receiver at a minimal loss [48, 49]. On the other hand, real-time control of the reflection amplitude and phase shift of RISs can present huge implementation issues [50]. In order to address

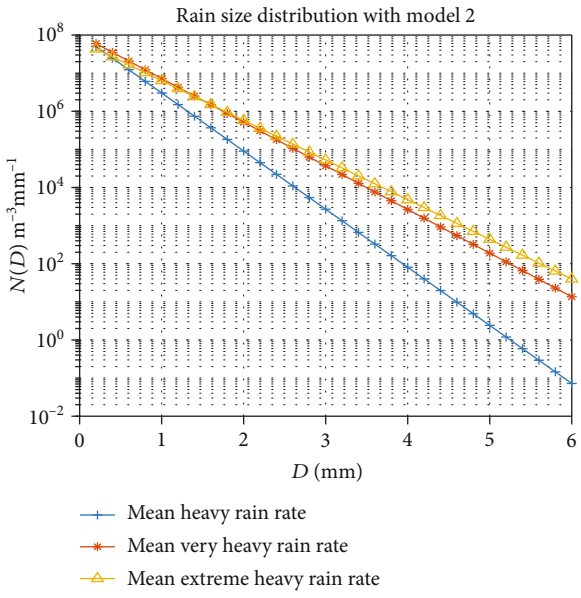

Figure 3: Raindrop size distribution evaluation with model 2.

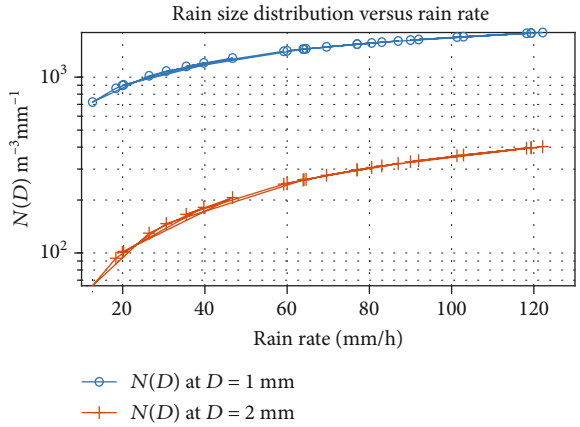

Figure 4: Connection between raindrop size and rain rate.

this problem, machine learning, deep learning, and federated learning models are currently proposed [51–53]. Testing and training data acquisition will limit machine learning-based RIS techniques [54, 55].

While a number of the reported attenuation studies are due to rain and microwave propagation data, such propagation attenuation levels information in the tropical region of Nigeria is still missing in the existing literature, especially at lower radio waves transmission frequencies. To this end, this study is designed to fill the gap in the open literature. In particular, the key contributions of the paper are as follows.

(i) We carried out realistic prognostic modeling of rain rate intensity levels based on 12-year experimental rainfall datasets

(ii) We classified the rainfall data into three clear groups based on the depth of rainfall in the region

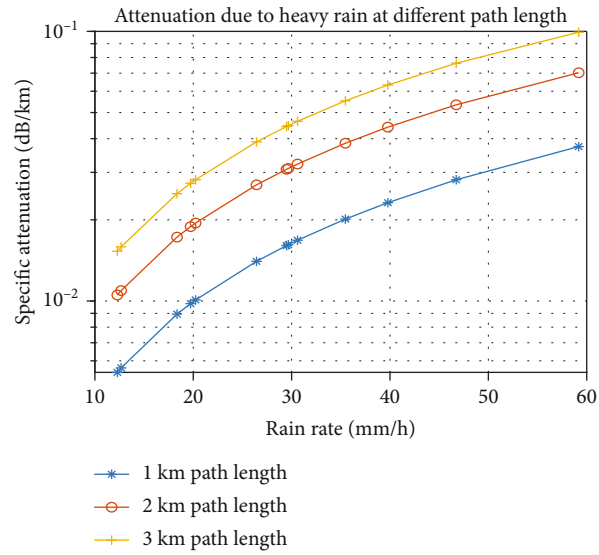

Figure 5: Specific attenuation due to heavy rainfall at different path lengths.

(iii) We estimated specific rain attenuation intensities in-depth on the 12-year rainfall data at 3.5 GHz microwave radio frequency

(iv) Establish the connection between the raindrop size and rain rate values

The remaining part of this paper is prepared as follows. The theoretical framework is defined in Section 2. The materials and methods comprising the study location, source of rainfall datasets collection method, and the stepwise procedure are briefed in Section 3. Section 4 presents the results and discussions, and a concise conclusion is drawn in Section 5.

2. Theoretical Framework

2.1. Specific Attenuation Model Based on Rec. ITU-R P.838-3 Power-Law. Specific attenuation S_r(dB/km) due to rainfall depth over a terrestrial communication channel can be articulated using the power-law relationship, which combines the propagation path length L_{path} (km) and rain rate R_r(mm/hr) given in equation (1), where γ is defined in equation (2) [22, 30]:

$$S_r = \gamma L_{\text{path}}, \tag{1}$$

where

$$\gamma = \beta(R_r)^{\alpha}. \tag{2}$$

The propagation path length L_{path} (km) can be obtained by multiplying the real channel length (l) with a distance parameter, d, and it is expressed in the following equation

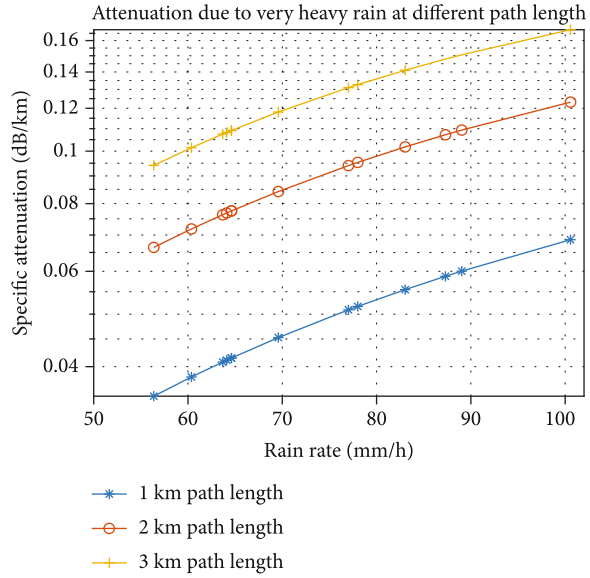

Figure 6: Specific attenuation due to very heavy rainfall at different path lengths.

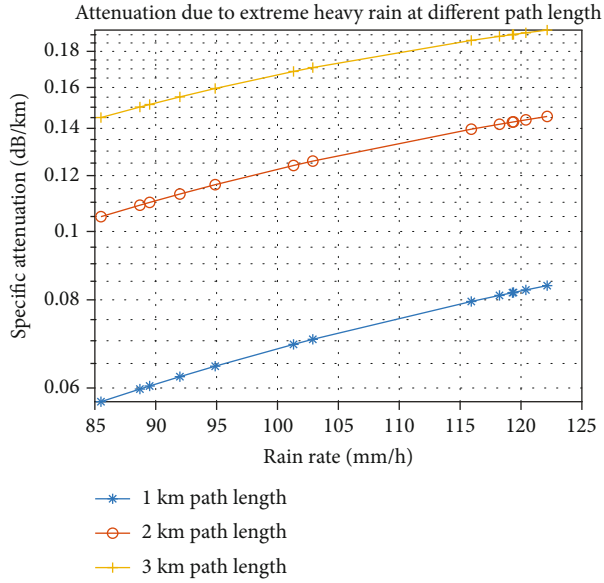

Figure 7: Specific attenuation due to extremely heavy rainfall at different path lengths.

[28, 56]:

$$d = \frac{1}{0.477 l^{0.633} R_r^{0.073\nu} f_c^{0.123} - 10.579(1 - \exp(-0.024 l))^{\alpha}}, \tag{3}$$

where ν indicates the specific attenuation regression constant.

The modeling parameters β and α can be obtained from the scattering calculation method in combination with curve

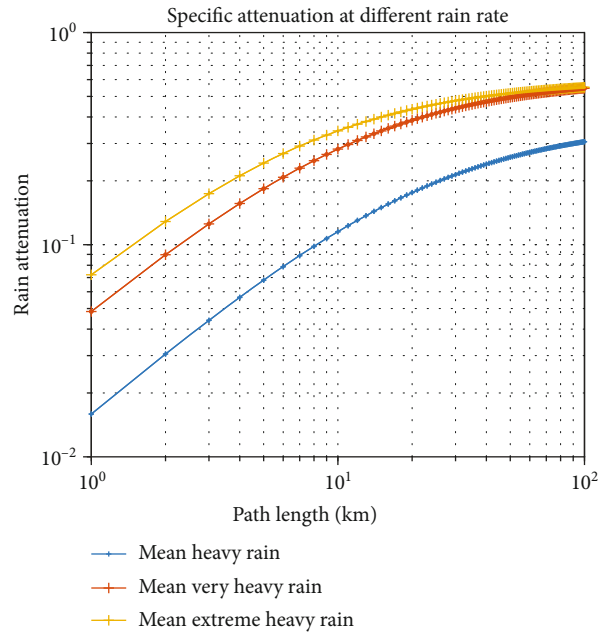

Figure 8: Specific attenuation versus path lengths of different rainfall depths.

fitting given in the following equations [30]:

$$\log \beta = \sum_{j=1}^{4} \left(x_j \exp\left[-\left(\frac{\log f_c - y_j}{z_j} \right)^2 \right] \right) + m_k \log f_c + z_k, \tag{4}$$

$$\log \alpha = \sum_{j=1}^{5} \left(x_i \exp\left[-\left(\frac{\log f_c - y_i}{z_i} \right)^2 \right] \right) + m_n \log f_c + z_n. \tag{5}$$

The rain attenuation $A_p(\mathrm{dB})$ exceeded at time percent, p in the range of 0.001–1% is expressed as given in the following equation:

$$A_p = A_{0.01} \left(\frac{p}{0.01} \right)^{-t_1 - t_2 n(A_{0.01}) - \beta(1-p)\sin\theta}, \tag{6}$$

where θ is the elevation angle and the time t_1 and t_2 are defined in the following equations, respectively.

$$t_1 = 0.655 + 0.033 \ln(p), \tag{7}$$

$$t_2 = 0.045. \tag{8}$$

The expression in equation (2) defines the popular power-law Rec. ITU-R P.838-3 for specific rain attenuation modeling.

2.2. Rain Drop Size Distribution Modeling and Connection with Rain Rate. Rainfall occurrence primarily expresses the wide-ranging formation of raindrop sizes [57–60]. Raindrop size distribution (DSD) describes the composition or

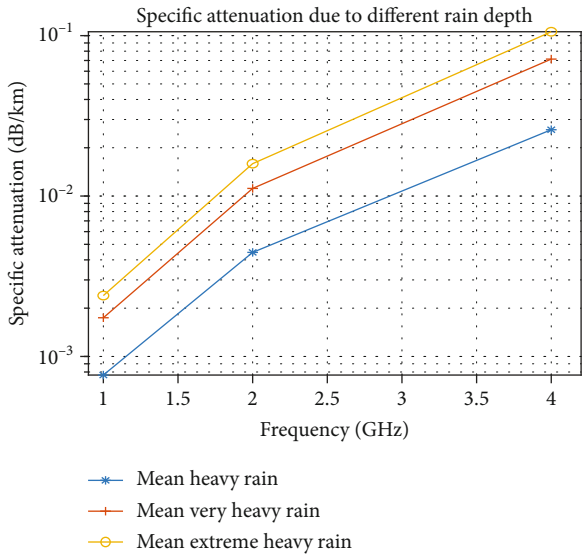

Figure 9: Specific attenuation versus frequency of different rainfall depths.

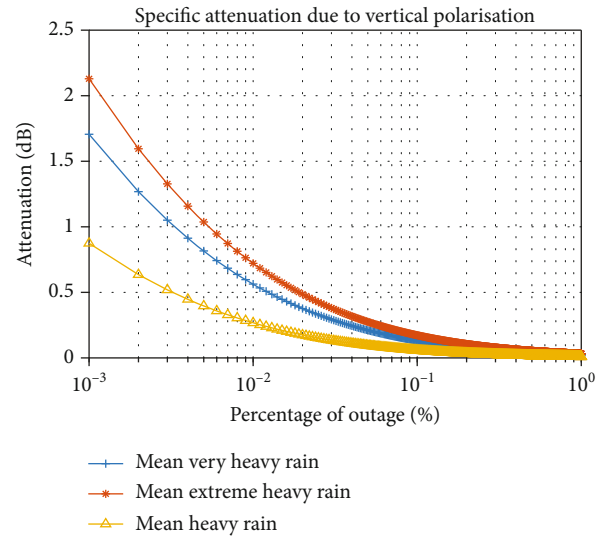

Figure 10: Specific attenuation versus time percentage due to vertical polarisation.

formation variant of diverse raindrop sizes (number) based on their diameter (D). Information on predictive modeling of DSD is vital for the robust evaluation and classification of radio and microwaves propagation effects in space. It also provides valuable information on the general microphysics composition of the precipitation phenomenon [61, 62].

There are many DSD models in the literature to analyse and evaluate rainfall events. In this paper, the two most popular ones with simplified computation convolution are considered, both of which are tagged model 1 and model 2 as described in equations (9), (10), (11), and (12).

$$N(D) = N_i D^a \exp\left(-\Lambda_s D^b\right), \tag{9}$$

$$N_i = 1.76 \times 10^6 R_r^{-1.2}, \tag{10}$$

$$\Lambda_s = 10 R_r^{-0.31}, \tag{11}$$

where $N(D)$ indicate the raindrop size number, with N_i and Λ_s being the modeling intercept parameter and slope parameter. a and b are also $N(D)$ modeling parameters where R_r and D indicate the raindrop diameter and rain rate. For $a = 0$ and $q = 1$, the expression in (1) turns

$$N(D) = N_i \exp\left(-\Lambda_s D\right). \tag{12}$$

While equation (4) explains the popular model developed by Marshall and Palmer [63] for raindrop size modeling, equation (1) describes the general form of the raindrop size model developed by proposed Ulbrich [64] to take into account a larger range of D values.

3. Materials and Methods

This section describes the study area, data collection method, and the methodology employed in this study.

3.1. Study Area. Kogi state, a midcentral (middle belt) zone of Nigeria, is a case study for the research work. Kogi, which connotes "River" in the Hausa language, houses a confluence town, where River Niger and Benue meet. The region holds a tropical climate with inconstant dry and rainy seasons in duration, timing, and severity. Despite the region's relatively irregular dry and rainy seasons, the total annual rainfall depth varies between 805 mm and 1767 mm. It is a tropical region of Nigeria with low humidity of about 30% in the dry season and high humidity of approximately 70% during the wet season [65, 66]. The rainy wet season of the region usually brings cooler weather, mainly due to cloud cover increase that most time acts as a blockage to the intense tropical sunshine. However, during afternoons, this season can be as hot and humid due to the surrounding rocky soils and the riverine nature of the area. During dry seasons, the sun shines over the expanse with little or no blockades from the atmosphere, thus making the season in the region a period of hot and warm temperature conditions [67]. But in the mid-dry season, which is usually around December/January, the hot sun's rays are partly blocked by the Harmattan haze and dust, which often results in lower temperatures. Its annual temperature is ranged between 27.7°C and 37.7°C in the wet and dry seasons. The average daily vapour pressure and wind speeds are 26 Hpa and 89.9 km/hr.

3.2. Data Collection. The 12-year rainfall datasets explored for this study were acquired with support from the Lokoja zone of the Nigerian Meteorological Agency (NIMET). It is the primary agency of the Nigerian government equipped with relevant meteorological facilities to collect the bulk of daily, monthly, and yearly data on weather and climate data. The agency has branches located in the 36 state capitals, Nigeria. The 12-year rainfall datasets ranged from 1st January 2008 to 31st December 2020. The datasets comprised the bulk of daily, monthly, and yearly rainfall amounts. Remarkably, such long-term datasets were engaged to thoroughly examine and make known the steadiness of the

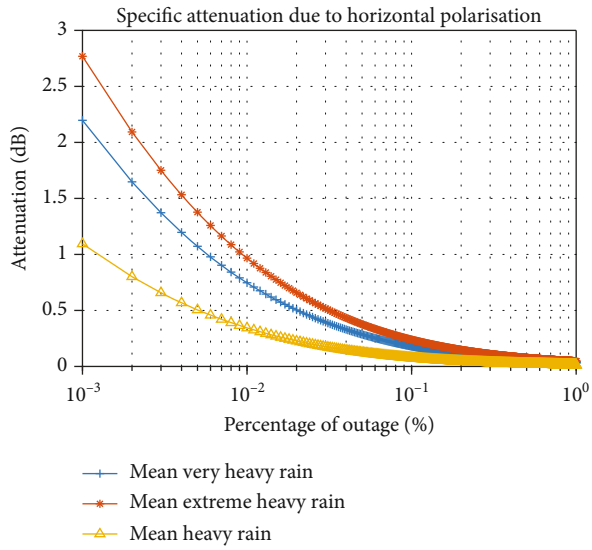

Figure 11: Specific attenuation versus time percentage due to horizontal polarisation.

Table 1: Statistics of rain rates due to different rain depth.

Statistics	Rain rate due to heavy rainfall	Rain rate due to very heavy rainfall	Rain rate due to extremely heavy rainfall
Mean	29.27	73.71	100.39
Minimum	12.28	60.36	85.50
Maximum	59.18	100.57	122.15
Moment	12.28	60.36	85.50
Kurtosis	2.90	2.25	1.13
Skewness	0.71	0.56	-0.10

bearing effect of the rainfall amount and their attenuation level effects in the study location, especially about microwaves radio frequency cellular communication links.

3.3. Stepwise Procedure. This work employs a practical based stepwise method to actualize the research aim. The practical based stepwise methodology is highlighted:

(i) Obtain the rainfall data and its related modeling parameters

(ii) Convert the rainfall data to rain rate using the expression in the following equation

$$R_r = L_m \frac{60}{T}, \tag{13}$$

where T and L_m indicate the rainfall time interval in min and rainfall depth in mm. The R_r defines the rain rate.

(iii) Explore the theoretical specific framework for the rain attenuation model, provided in detail in Section 2

(iv) Engage the calculated rain rate values with the power-law ITU-R model [56] (see equation (2)) to determine the specific attenuation levels for the study location

(v) Compute the rain rate intensity attenuation levels for different time percentages in the range of 0.001–1% (see equation (6))

(vi) Examine the effect of different microwave radio propagation path lengths on the specific attenuation levels

(vii) Establish the connection between the rain rate values and the specific attenuation values

(viii) Examine the effect of different horizontal and vertical polarisation on specific attenuation levels

(ix) Establish the connection between the raindrop size and rain rate values

4. Results and Discussions

The specific attenuation results are presented and discussed in this section. The results are obtained using a combination of the acquired 12-year rainfall dataset together with the ITU-R power law-based model and the rain rate conversion models, as expressed in equations (1), (2), (3), and (4). All the graphical results displayed (Figures 1–11) are plotted using MATLAB. First, the rainfall datasets were divided into three components based on their depth amount in mm. These include heavy, heavy, and extremely heavy, ranging from 10-59 mm, 60-89 mm, and 90-130 mm. The heavy rain depth falls from October to November, while very heavy and extremely heavy rains are obtained between April to June and July to September. Figure 1 and Table 1 display the cumulative distribution of the computed rain values due to the three classes of rain depths. The three rainfall classes produced average rain rates of about 29.27 mm/hr, 73.71 mm/hr, and 105.39 mm/hr during the investigation. Higher rain depths result in larger rain rate intensities from Table 1 and vice versa. For example, while heavy rain depth produced a 59.18 mm/hr maximum rain rate, 100.57 and 122.15 maximum rain rate values were attained due to very heavy rain and extremely heavy rain depths. Similarly, while heavy rain depth recorded a 12.28/hr minimum rain rate, 60.36 and 80.50 minimum rain rate values were achieved for the very heavy rain and extremely heavy rain depths.

Employing models 1 and 2, Figures 2 and 3 display the resultant logarithm sales of DSDs versus linear values of D for the three different rain rate classes averaged over 12 months. The significant difference between models 1 and 2 is that the latter considers more modeling parameters and a more extensive range of D values than the former, as revealed in equations (12) and (9). The results in the two graphs indicate that more significant rain rates values are composed of a higher dimension of raindrop diameters than lower rain rates. Remarkably, both DSD results attained maximum divergence at higher raindrop diameters.

Figures 2 and 3 suggest that $N(D)$ depends on rain rates and D and other climatic parameters like rainfall type.

Figure 4 provides graphical information on the connection between raindrop size and rain rate at diameter $D = 1$ mm and $D = 2$ mm, respectively. A gradual increase in rain rate (intensity) at lower values is seen in the graph as the distribution rainfall sizes become higher and more expansive. However, the gradual increase becomes slower and tends to logarithm stability at larger peak rain rate values of 100-120 mm h −1. This trend may suggest that the $N(D)$ may reach an equilibrium state at higher rain rates. Attaining an equilibrium state at higher rain rates agrees with the results of other authors in [68–71] that a peak $N(D)$ value is attained in correspondence with specific rain rates, wherein the raindrop sizes either become stable or fall subsequently. It is also clear from Figure 4 that the $N(D)$ results are mainly dependent on D sizes and the model engaged for its distributive analysis.

Figures 5–7 display the prognostic specific attenuation versus rain rate values at different path lengths for heavy, heavy, and extremely heavy rainfall depths. For higher rainfall rate values at higher path lengths, the aggregate atmospheric attenuation also rises steadily with heavy, very heavy, and extremely heavy rainfall depths. Higher rainfall depths lead to higher attenuation of propagated microwaves radio signals due to more signal scattering and absorption between the communication paths.

Figure 8 displays the computed rain-specific attenuation levels against different communication path lengths and rain depth for the study location. A quick observation from Figure 8 shows almost a direct relationship between specific attenuation levels and the communication path lengths. This trend indicates that increased communication paths between the transmitter and receiver would yield higher attenuation values due to path obstructions, especially where scattering and rain absorption are key components.

Figure 9 shows the computed rain-specific attenuation levels against frequency at different rain depth amounts for the study location. A key observation from Figure 9 shows a noticeable rise in attenuation values between 1 and 2 GHz and then drops a little as the frequency range increase. This trend reveals that signal transmission at higher frequencies would undoubtedly be more degraded by rain attenuation in the investigated area. Higher attenuation values were observed in Figure 9 for higher rainfall depths, which can be ascribed to more signal scattering and absorption as the raindrop increases.

Now, consider Figures 10 and 11 that display the rain attenuation amount computed at different percentages of time for horizontal and vertical polarisations under the three rain depth classes, respectively. The rain attenuation decreases gradually for higher time percentages, stretching up to 0.89 dB, 1.71 dB, and 2.13 dB for vertical polarisation and 1.09 dB, 1.20 dB, and 2.78 dB horizontal polarisation, respectively. These values show that higher rain attenuation is observed for horizontal polarisation compared to vertical polarisation. Specifically, horizontal polarisation has a higher 12% attenuation value than vertical polarisation.

5. Conclusions

Signal propagation at different radio waves and microwave carrier frequencies in terrestrial point-to-point and Earth-space satellite communication links is greatly influenced by precipitation, principally rain. Thus, attenuation effects based on different atmospheric conditions must be investigated and quantified for effective design and efficient deployment of communication links. The current contribution explores a 12-year rainfall dataset to conduct realistic prognostic modeling of rain rate amount and specific rain attenuation intensity levels at 3.5 GHz. The atmospheric attenuation-based predictive modeling has been achieved by combining the ITU-R model with the experimental 60-minute intervals of rainfall data measured from 2008 to 2020. The rainfall datasets were classified into three components based on their depth amount in mm. These are heavy rain, very heavy rain, and extremely heavy rain, all of which ranged from 10-59 mm, 60-89 mm, and 90-130 mm, respectively. On average, the three rainfall classes produced rain rates of about 29.27 mm/hr, 73.71 mm/hr, and 105.39 mm/hr, respectively. The corresponding attenuation values are 0.89 dB, 1.71 dB, and 2.13 dB for vertical polarisation and 1.09 dB, 1.20 dB, and 2.78 dB horizontal polarisation, and both occurred at 0.01% time percentage computation. Our future work would focus on optimizing the projected rain rate models for improved performance.

Data Availability

The data that support the findings of this study are available from the corresponding author upon reasonable request.

Conflicts of Interest

The authors declare that they have no conflicts of interest.

Acknowledgments

The authors thank King Khalid University, Saudi Arabia, for partially supporting this work through the King Khalid University Researchers Supporting Project Number (R. G. P. 1/85/42). Also, the authors thank the Nigerian Meteorological Agency (NIMET) for the atmospheric dataset acquisition and other relevant guidance provided to accomplish this research work. The work of Agbotiname Lucky Imoize is partially supported by the Nigerian Petroleum Technology Development Fund (PTDF) and the German Academic Exchange Service (DAAD) through the Nigerian-German Postgraduate Program under Grant 57473408.

References

[1] J. Isabona and A. L. Imoize, "Terrain-based adaption of propagation model loss parameters using non-linear square regression," *Journal of Engineering and Applied Science*, vol. 68, no. 1, pp. 1–19, 2021.

[2] D. O. Ojuh and J. Isabona, "Field electromagnetic strength variability measurement and adaptive prognostic approximation with weighed least regression approach in the ultra-high radio

frequency band," *International Journal of Intelligent Systems & Applications*, vol. 13, no. 4, 2021.

[3] J. Isabona, "Wavelet generalized regression neural network approach for robust field strength prediction," *Wireless Personal Communications*, vol. 114, no. 4, pp. 3635–3653, 2020.

[4] V. C. Ebhota, J. Isabona, and V. M. Srivastava, "Environment-adaptation based hybrid neural network predictor for signal propagation loss prediction in cluttered and open urban microcells," *Wireless Personal Communications*, vol. 104, no. 3, pp. 935–948, 2019.

[5] A. L. Imoize, E. M. Otuokere, S. O. Ajose, and A. O. Adegbenro, "Experimental validation of a best-fit model for predicting radio wave propagation through vegetation," *Arid Zone Journal of Engineering, Technology and Environment*, vol. 15, pp. 172–186, 2019.

[6] S. Joshi, S. Stalin, P. K. Shukla et al., "Unified authentication and access control for future mobile communication- based lightweight IoT systems using blockchain," *Wireless Communications and Mobile Computing*, vol. 2021, 12 pages, 2021.

[7] G. U. Ughegbe, M. A. Adelabu, and A. L. Imoize, "Experimental data on radio frequency interference in microwave links using frequency scan measurements at 6 GHz, 7 GHz, and 8 GHz," *Data Br.*, vol. 35, article 106916, 2021.

[8] M. A. Adelabu, A. L. Imoize, and G. U. Ughegbe, "Performance evaluation of radio frequency interference measurements from microwave links in dense urban cities," *Telecom*, vol. 2, no. 4, pp. 328–368, 2021.

[9] B. Butani, P. K. Shukla, and S. Silakari, "An exhaustive survey on physical node capture attack in WSN," *International Journal of Computer Applications*, vol. 95, no. 3, 2014.

[10] O. O. Ometan, T. V. Omotosho, M. O. Adewusi, and S. A. Akinwumi, "Evaluation of the variation in wind speed during rainfall in a tropical location," *IOP Conference Series: Earth and Environmental Science*, vol. 655, no. 1, p. 12057, 2021.

[11] Z. A. Shamsan and A. Al-Saman, "Performance of the DBS satellite receiver under the impact of rainfall and terrestrial interference," *Wireless Communications and Mobile Computing*, vol. 2021, 12 pages, 2021.

[12] A. Y. Alhilal, T. Braud, and P. Hui, "A roadmap toward a unified space communication architecture," *IEEE Access*, vol. 9, pp. 99633–99650, 2021.

[13] N. K. Rathore, N. K. Jain, P. K. Shukla, U. Rawat, and R. Dubey, "Image forgery detection using singular value decomposition with some attacks," *National Academy Science Letters*, vol. 44, no. 4, pp. 331–338, 2021.

[14] A. Y. Abdulrahman, T. A. Rahman, B. J. Olufeagba, and M. D. R. Islam, "Using full rainfall rate distribution for rain attenuation predictions over terrestrial microwave links in Malaysia," *Signal Process. Res*, vol. 2, no. 1, pp. 25–28, 2013.

[15] L. Luini and C. Capsoni, "A unified model for the prediction of spatial and temporal rainfall rate statistics," *IEEE Transactions on Antennas and Propagation*, vol. 61, no. 10, pp. 5249–5254, 2013.

[16] L. Mello and M. S. Pontes, "Unified method for the prediction of rain attenuation in satellite and terrestrial links," *Journal of Microwaves, Optoelectronics and Electromagnetic Applications*, vol. 11, no. 1, pp. 01–14, 2012.

[17] A. L. Imoize, K. Orolu, and A. A.-A. Atayero, "Analysis of key performance indicators of a 4G LTE network based on experimental data obtained from a densely populated smart city," *Data in brief*, vol. 29, no. 105304, pp. 1–17, 2020.

[18] A. L. Imoize and O. D. Adegbite, "Measurements-based performance analysis of a 4G LTE network in and around shopping malls and campus environments in Lagos Nigeria," *Arid Zone Journal of Engineering, Technology and Environment*, vol. 14, no. 2, pp. 208–225, 2018.

[19] A. L. Imoize and T. E. Ogunfuwa, "Propagation measurements of a 4G LTE network in lagoon environment," *Nigerian Journal of Technological Development*, vol. 16, no. 1, pp. 1–9, 2019.

[20] J. O. Ogbebor, A. L. Imoize, and A. A.-A. Atayero, "Energy efficient design techniques in next-generation wireless communication networks: emerging trends and future directions," *Wireless Communications and Mobile Computing*, vol. 2020, Article ID 7235362, 19 pages, 2020.

[21] G. Khambra and P. Shukla, "Novel machine learning applications on fly ash based concrete: an overview," *Materials Today: Proceedings*, 2021.

[22] M. Ekpenyong, E. Umoren, and J. Isabona, "A rain attenuation model for predicting fading effect on wireless communication systems in the tropics," *Nigerian Journal of Space Research*, vol. 6, pp. 21–32, 2009.

[23] O. Goldshtein, H. Messer, and A. Zinevich, "Rain rate estimation using measurements from commercial telecommunications links," *IEEE Transactions on Signal Processing*, vol. 57, no. 4, pp. 1616–1625, 2009.

[24] K. P. S. Sudarshana and A. Samarasinghe, "Rain rate and rain attenuation estimation for Ku band satellite communications over Sri Lanka," in *2011 6th International Conference on Industrial and Information Systems*, pp. 1–6, 2011.

[25] F. Giannetti, R. Reggiannini, M. Moretti et al., "Real-time rain rate evaluation via satellite downlink signal attenuation measurement," *Sensors*, vol. 17, no. 8, p. 1864, 2017.

[26] F. J. A. Andrade, Á. A. M. de Medeiros, and L. A. R. da Silva Mello, "Short-term rain attenuation predictor for terrestrial links in tropical area," *IEEE Antennas and Wireless Propagation Letters*, vol. 16, pp. 1325–1328, 2016.

[27] L. Luini and C. Capsoni, "The SC EXCELL model for prediction of rain attenuation on terrestrial radio links," *Electronics Letters*, vol. 49, no. 4, pp. 307-308, 2013.

[28] F. D. Diba, T. J. Afullo, and A. A. Alonge, "Rainfall rate and attenuation performance analysis at microwave and millimeter bands for the design of terrestrial line-of-sight radio links in Ethiopia," *SAIEE Africa Research Journal*, vol. 107, no. 3, pp. 177–186, 2016.

[29] M. C. Kestwal, S. Joshi, and L. S. Garia, "Prediction of rain attenuation and impact of rain in wave propagation at microwave frequency for tropical region (Uttarakhand, India)," *International Journal of Microwave Science and Technology*, vol. 2014, Article ID 958498, 6 pages, 2014.

[30] A. Maitra, "Rain attenuation modeling from measurements of rain drop size distribution in the Indian region," *IEEE Antennas and Wireless Propagation Letters*, vol. 3, no. 1, pp. 180-181, 2004.

[31] Y. B. Kaya and Ü. C. YILMAZ, "Rain rate and rain attenuation prediction for satellite communication in Ku band beacon over TURKSAT Golbası," *Sakarya University Journal of Computer and Information Sciences*, vol. 4, no. 3, pp. 354–359, 2021.

[32] N. Elfadil, Z. Nadir, A. Salam, and J. Rao, "Microwave attenuation studies due to rain for communication links operating in Malaysia," *Computer Science and Telecommunications*, vol. 1, pp. 9–17, 2005.

[33] A. Hirata, R. Yamaguchi, H. Takahashi et al., "Effect of rain attenuation for a 10-Gb/s 120-GHz-band millimeter-wave wireless link," *IEEE transactions on microwave theory and techniques*, vol. 57, no. 12, pp. 3099–3105, 2009.

[34] S. Shrestha and D.-Y. Choi, "Rain attenuation statistics over millimeter wave bands in South Korea," *Journal of Atmospheric and Solar-Terrestrial Physics*, vol. 152-153, pp. 1–10, 2017.

[35] F. Norouzian, E. Marchetti, M. Gashinova et al., "Rain attenuation at millimeter wave and low-THz frequencies," *IEEE Transactions on Antennas and Propagation*, vol. 68, no. 1, pp. 421–431, 2020.

[36] S. Pérez-Pena, J. M. Riera, A. Benarroch, D. Pimienta-del-Valle, and P. Garcia-del-Pino, "Variability of rain attenuation in the 100-200 GHz band calculated from experimental drop size distributions," in *2021 15th European Conference on Antennas and Propagation (EuCAP)*, pp. 1–5, 2021.

[37] J. M. Riera, A. Benarroch, P. Garcia-del-Pino, and S. Pérez-Peña, "Preprocessing and assessment of rain drop size distributions measured with a K-band Doppler radar and an optical disdrometer," *IEEE Transactions on Instrumentation and Measurement*, vol. 70, pp. 1–8, 2021.

[38] L. Morais, L. Menezes, and P. Moraes, "Rain attenuation at THz frequencies from historical data collected in Brasilia, Brazil," in *2021 USNC-URSI Radio Science Meeting (USCN-URSI RSM)*, pp. 45–50, 2021.

[39] W. Tashan, I. Shayea, S. Aldirmaz-Colak, T. A. Rahman, A. A. El-Saleh, and M. Roslee, "Rain rate and rain attenuation over millimeter waves in tropical regions based on real measurements," in *2021 IEEE 15th Malaysia International Conference on Communication (MICC)*, pp. 120–125, 2021.

[40] R. Ghiani, L. Luini, and A. Fanti, "A physically based rain attenuation model for terrestrial links," *Radio Science*, vol. 52, no. 8, pp. 972–980, 2017.

[41] A. I. O. Yussuff and N. H. H. Khamis, "Modified ITU-R rain attenuation prediction model for a tropical station," *Journal of Industrial and Intelligent Information*, vol. 1, no. 3, 2013.

[42] F. A. Semire, R. Mohd-Mokhtar, W. Ismail, N. Mohamad, and J. S. Mandeep, "Modeling of rain attenuation and site diversity predictions for tropical regions," *Annales Geophysicae*, vol. 33, no. 3, pp. 321–331, 2015.

[43] H. Singh, V. Kumar, K. Saxena, B. Boncho, and R. Prasad, "Proposed model for radio wave attenuation due to rain (RWAR)," *Wireless Personal Communications*, vol. 115, no. 1, pp. 791–807, 2020.

[44] A. G. Ashidi, J. S. Ojo, O. J. Ajayi, and T. M. Akinmoladun, "Evaluation of concurrent variation in rain specific attenuation and tropospheric amplitude scintillation over Akure, Southwest Nigeria," *Earth Systems and Environment*, vol. 5, no. 3, pp. 547–559, 2021.

[45] H. Han, J. Zhao, D. Niyato, M. Di Renzo, and Q. V. Pham, "Intelligent reflecting surface aided network: power control for physical-layer broadcasting," in *IEEE International Conference on Communications*, 2020.

[46] Q. Wu and R. Zhang, "Intelligent reflecting surface enhanced wireless network via joint active and passive beamforming," *IEEE Transactions on Wireless Communications*, vol. 18, no. 11, pp. 5394–5409, 2019.

[47] Q. Wu and R. Zhang, "Towards smart and reconfigurable environment: intelligent reflecting surface aided wireless network," *IEEE Communications Magazine*, vol. 58, no. 1, pp. 106–112, 2020.

[48] A. L. Imoize, O. Adedeji, N. Tandiya, and S. Shetty, "6G enabled smart infrastructure for sustainable society: opportunities, challenges, and research roadmap," *Sensors*, vol. 21, no. 5, pp. 1–58, 2021.

[49] M. Diamanti, P. Charatsaris, E. E. Tsiropoulou, and S. Papavassiliou, "The prospect of reconfigurable intelligent surfaces in integrated access and backhaul networks," *IEEE Transactions on Green Communications and Networking*, 2021.

[50] S. Zhou, W. Xu, K. Wang, M. Di Renzo, and M. S. Alouini, "Spectral and energy efficiency of IRS-assisted MISO communication with hardware impairments," *IEEE Wireless Communications Letters*, vol. 9, no. 9, pp. 1366–1369, 2020.

[51] A. Taha, M. Alrabeiah, and A. Alkhateeb, "Enabling large intelligent surfaces with compressive sensing and deep learning," *IEEE Access*, vol. 9, pp. 44304–44321, 2021.

[52] Z. Qin, H. Ye, G. Y. Li, and B. H. F. Juang, "Deep learning in physical layer communications," *IEEE Wireless Communications*, vol. 26, no. 2, pp. 93–99, 2019.

[53] Z. Yang, M. Chen, K.-K. Wong, H. V. Poor, and S. Cui, *Federated Learning for 6G: Applications, Challenges, and Opportunities*, pp. 1–23, 2021, Available: http://arxiv.org/abs/2101.01338.

[54] S. Ojo, A. Imoize, and D. Alienyi, "Radial basis function neural network path loss prediction model for LTE networks in multitransmitter signal propagation environments," *International Journal of Communication Systems*, vol. 34, no. 3, p. e4680, 2021.

[55] S. Ojo, M. Akkaya, and J. C. Sopuru, "An ensemble machine learning approach for enhanced path loss predictions for 4G LTE wireless networks," *International Journal of Communication Systems*, vol. 35, no. 7, Article ID e5101, 2022.

[56] ITU-R, "Propagation data and prediction methods required for the design of terrestrial line-of-sight systems," *Recommendation ITU-R*, pp. 512–530, 2015.

[57] M. L. Yakubu, Z. Yusop, and F. Yusof, "The modelled raindrop size distribution of Skudai, Peninsular Malaysia, using exponential and lognormal distributions," *Scientific World Journal*, vol. 2014, article 361703, 7 pages, 2014.

[58] A. C. Best, "The size distribution of raindrops," *Quarterly Journal of the Royal Meteorological Society*, vol. 76, no. 327, pp. 16–36, 1950.

[59] A. P. Barros, O. P. Prat, and F. Y. Testik, "Size distribution of raindrops," *Nature Physics*, vol. 6, no. 4, p. 232, 2010.

[60] E. Villermaux and B. Bossa, "Size distribution of raindrops," *Nature Physics*, vol. 6, no. 4, p. 232, 2010.

[61] R. Uijlenhoet and J. N. M. Stricker, "A consistent rainfall parameterization based on the exponential raindrop size distribution," *Journal of Hydrology*, vol. 218, no. 3–4, pp. 101–127, 1999.

[62] P. Hazenberg, H. Leijnse, and R. Uijlenhoet, "The impact of reflectivity correction and accounting for raindrop size distribution variability to improve precipitation estimation by weather radar for an extreme low-land mesoscale convective system," *Journal of Hydrology*, vol. 519, pp. 3410–3425, 2014.

[63] J. S. Marshall and W. M. K. Palmer, "The distribution of raindrops with size," *Journal meteor*, vol. 5, no. 4, pp. 165-166, 1948.

[64] C. W. Ulbrich, "Natural variations in the analytical form of the raindrop size distribution," *Journal of Climate and Applied Meteorology*, vol. 22, no. 10, pp. 1764–1775, 1983.

[65] M. H. Sani and U. Haruna, "arm planning model for sustainable vegetable crop production in the eastern part of Kogi State, Nigeria," *Journal of Agronomy*, vol. 9, no. 1, pp. 17–22, 2009.

[66] U. A. Saleh, Y. S. Haruna, S. M. Isa, and S. A. Jumaat, "Statistical evaluation of wind speed data for power generation at Anyigba, Kogi State, Nigeria," in *Proceedings of the 12th National Technical Seminar on Unmanned System Technology 2020*, pp. 1091–1101, 2022.

[67] I. O. Oluseyi and A. J. Olusegun, "Managing land use transformation and land surface temperature change in Anyigba Town, Kogi State, Nigeria," *Journal of Geography and Geology*, vol. 3, no. 1, p. 77, 2011.

[68] F. G. Carollo, V. Ferro, and M. A. Serio, "Estimating rainfall erosivity by aggregated drop size distributions," *Hydrological Processes*, vol. 30, no. 13, pp. 2119–2128, 2016.

[69] D. T. Meshesha, A. Tsunekawa, and N. Haregeweyn, "Influence of raindrop size on rainfall intensity, kinetic energy, and erosivity in a sub-humid tropical area: a case study in the northern highlands of Ethiopia," *Theoretical and Applied Climatology*, vol. 136, no. 3-4, pp. 1221–1231, 2019.

[70] P. Pateriya, R. Singhai, and P. Shukla, "Design and implementation of optimum LSD coded signal processing algorithm in the multiple-antenna system for the 5G wireless technology," *Wireless Communications and Mobile Computing*, vol. 2022, Article ID 7628814, 12 pages, 2022.

[71] N. Jain, S. Rathore, and P. K. Shukla, "Designing efficient optimum reduced order IIR filter for smoothening EEG motion artifacts signals," *Design Engineering*, pp. 5080–5101, 2021.